Dose optimization of intrathecal administration of human umbilical cord mesenchymal stem cells for the treatment of subacute incomplete spinal cord injury

https://doi.org/10.4103/1673-5374.332151

Date of submission: February 20, 2021

Date of decision: May 13, 2021

Date of acceptance: November 10, 2021

Date of web publication: January 7, 2022

Ting-Ting Cao[1, #], Huan Chen[1, #], Mao Pang[2, 3, 4, #], Si-Si Xu[1], Hui-Quan Wen[5], Bin Liu[2, 3, 4, *], Li-Min Rong[2, 3, 4, *], Mang-Mang Li[1, *]

From the Contents

Graphical Abstract *Efficacy studies of intrathecal implantation of human umbilical cord mesenchymal stem cells in a rodent model of spinal cord injury*

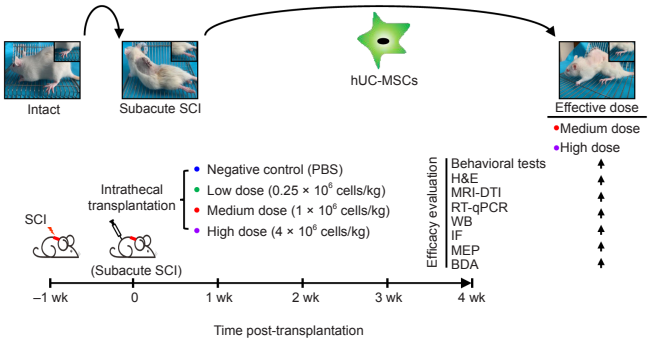

Abstract

Human umbilical cord mesenchymal stem cells (hUC-MSCs) are a promising candidate for spinal cord injury (SCI) repair owing to their advantages of low immunogenicity and easy accessibility over other MSC sources. However, modest clinical efficacy hampered the progression of these cells to clinical translation. This discrepancy may be due to many variables, such as cell source, timing of implantation, route of administration, and relevant efficacious cell dose, which are critical factors that affect the efficacy of treatment of patients with SCI. Previously, we have evaluated the safety and efficacy of 4×10^6 hUC-MSCs/kg in the treatment of subacute SCI by intrathecal implantation in rat models. To search for a more accurate dose range for clinical translation, we compared the effects of three different doses of hUC-MSCs – low (0.25×10^6 cells/kg), medium (1×10^6 cells/kg) and high (4×10^6 cells/kg) – on subacute SCI repair through an elaborate combination of behavioral analyses, anatomical analyses, magnetic resonance imaging-diffusion tensor imaging (MRI-DTI), biotinylated dextran amine (BDA) tracing, electrophysiology, and quantification of mRNA levels of ion channels and neurotransmitter receptors. Our study demonstrated that the medium dose, but not the low dose, is as efficient as the high dose in producing the desired therapeutic outcomes. Furthermore, partial restoration of the γ-aminobutyric acid type A ($GABA_A$) receptor expression by the effective doses indicates that $GABA_A$ receptors are possible candidates for therapeutic targeting of dormant relay pathways in injured spinal cord. Overall, this study revealed that intrathecal implantation of 1×10^6 hUC-MSCs/kg is an alternative approach for treating subacute SCI.

Key Words: effective dose; human umbilical cord mesenchymal stem cells; intrathecal implantation; ion channels; neurotransmitter receptors; spinal cord injury; subacute spinal cord injury; γ-aminobutyric acid type A ($GABA_A$) receptors

Introduction

The devastating effects of spinal cord injury (SCI) on the central nerves system (CNS), which has poor intrinsic regenerative capacity, result in temporary or permanent functional loss of sensory, locomotor, and autonomic systems, making it an incurable disease to date (Rao et al., 2018). Multiple obstacles, including the inability of damaged axons to form original circuits, the inhibitory inflammatory environment that surrounds the lesion site, and the glial scar

[1]Department of Cell Biology, School of Basic Medical Sciences, Southern Medical University, Guangzhou, Guangdong Province, China; [2]Department of Spine Surgery, The Third Affiliated Hospital of Sun Yat-sen University, Guangzhou, Guangdong Province, China; [3]Guangdong Provincial Center for Engineering and Technology Research of Minimally Invasive Spine Surgery, Guangzhou, Guangdong Province, China; [4]Guangdong Provincial Center for Quality Control of Minimally Invasive Spine Surgery, Guangzhou, Guangdong Province, China; [5]Department of Radiology, The Third Affiliated Hospital of Sun Yat-sen University, Guangzhou, Guangdong Province, China

*Correspondence to: Mang-Mang Li, PhD, mangmangli@smu.edu.cn; Bin Liu, MD, liubin6@mail.sysu.edu.cn; Li-Min Rong, PhD, ronglm@mail.sysu.edu.cn .
https://orcid.org/0000-0002-4182-6509 (Mang-Mang Li); https://orcid.org/0000-0003-0373-7393 (Li-Min Rong);
https://orcid.org/0000-0003-1882-318X (Bin Liu)
#These authors contributed equally to this work.

Funding: *This work was supported by the National Key Research and Development Program of China, No. 2017YFA0105401 (to LMR), the National Natural Science Foundation of China, Nos. 31671420 and 81602482 (to MML) and a grant from the Guangdong Provincial Key Laboratory of Bone and Joint Degeneration Diseases.*

How to cite this article: *Cao TT, Chen H, Pang M, Xu SS, Wen HQ, Liu B, Rong LM, Li MM (2022) Dose optimization of intrathecal administration of human umbilical cord mesenchymal stem cells for the treatment of subacute incomplete spinal cord injury. Neural Regen Res 17(8):1785-1794.*

formation, can pose great challenges for the functional recovery of the injured spinal cord (Fink and Cafferty, 2016; Fan et al., 2018; Yu and Gu, 2019). Human umbilical cord mesenchymal stem cells (hUC-MSCs) endowed with faster self-renewal and lower immunogenicity than other sources of MSCs hold great promise for SCI repair (Nagamura-Inoue and He, 2014; Liu et al., 2020). To our knowledge, the neuroprotective effect of hUC-MSCs on SCI is mainly through their paracrine activity that promotes revascularization, suppresses inflammation and apoptosis, and secretes neurotrophic factors that enhance the axonal regeneration (Torres-Espin et al., 2013; Zhilai et al., 2016; Shende and Subedi, 2017). Although encouraging results have been demonstrated in SCI experimental models, modest clinical efficacy hampered the progression of the clinical translation of hUC-MSCs (Cofano et al., 2019; Liau et al., 2020). This discrepancy may be due to many variables, such as cell source, timing of implantation, route of administration, and relevant efficacious cell dose, which are critical factors that affect the efficacy of treatment of patients with SCI. The transplanted cell doses are different according to the route of administration and the phase of SCI (Kabat et al., 2020; Silvestro et al., 2020). Although hUC-MSCs exhibit low immunogenicity after transplantation compared with other stem cells, the risk of possible immune reactions should always be considered. Our previous study has demonstrated that subarachnoid administration of 4×10^6 hUC-MSCs/kg in a rat model is a safe and efficacious strategy for subacute incomplete SCI treatment (Yang et al., 2020a). To minimize the unwanted side effects, maximize the functional potential, and design a standardized clinical study protocol, the range of effective doses of a given stem cell type for a certain route of administration remains to be thoroughly illustrated in animal models prior to the clinical translation. On the basis of these considerations, the present preclinical study aimed to find a therapeutic dose range for intrathecal administration of hUC-MSCs in a rat model of subacute incomplete SCI.

Materials and Methods

Ethics statement

Animal experiments were approved by the Institutional Animal Care and Use Committee of Southern Medical University (No. K2018018) on April 11, 2018) and conducted in strict accordance with international laws and National Institutes of Health (NIH) policies, including the Care and Use of Laboratory Animals (NIH publication No. 85-23, 1985, revised 1996). This study is reported in accordance with the ARRIVE 2.0 guidelines (Animal Research: Reporting of *In Vivo* Experiments) (Percie du Sert et al., 2020).

The use of hUC-MSCs was approved by the Stem Cell Clinical Trials Ethics Committee of the Third Affiliated Hospital of Sun Yat-sen University (No. 201804) on March 30, 2018. All procedures using primary human cells were under the supervision of Cell-Gene Therapy Translational Medicine Research Center in the Third Affiliated Hospital of Sun Yat-sen University. The study protocol, which included patients with subacute SCI that received intrathecal injection of hUC-MSCs and were recruited from the Third Affiliated Hospital of Sun Yat-sen University, was registered in ClinicalTrials.gov (Identifier: NCT03521336).

Isolation and expansion of hUC-MSCs

The hUC-MSC isolation procedure was performed in accordance with the methodology described by Davies et al. (Chen et al., 2015). Briefly, umbilical cords collected within 2 hours after birth were disinfected with 75% alcohol and washed with 0.9% normal saline. Two arteries and one vein within the umbilical cord were removed and the Wharton's Jelly was mechanically split into approximately 1 cm^3 fragments. The fragments were digested with a mixed enzyme solution consisting of 10 mg/mL collagenase type I (MilliporeSigma, Burlington, MA, USA) and 1.25 mg/mL hyaluronidase (MilliporeSigma) for approximately 3 hours. Undigested tissue was removed by filtration. The released cells were washed twice and cultured in hUC-MSC complete medium (Dulbecco's Modified Eagle's Medium [DMEM; Corning, New York, NY, USA] containing 10% fetal bovine serum [FBS], 1% glutamine, 1% Minimum Essential Medium [MEM], Nonessential Amino Acids, and penicillin/streptomycin). When the hUC-MSCs reached 80% confluency, they were passaged three times to obtain the highest purity fraction.

Induction of subacute incomplete SCI and cell transplantation

In total, 72 adult female Sprague-Dawley rats (~250 g body weight, 6–8 weeks old) were used and randomly assigned to six groups (Intact, SCI 7d, phosphate-buffered saline [PBS], low dose, medium dose, and high dose). The rat models of subacute incomplete SCI and intrathecal transplantation of hUC-MSCs were established as previously described (Yang et al., 2020b). Before surgery, all rats were acclimatized to the housing facility, which was kept at 18–29°C and 40–70% humidity, for 4 days. To generate the incomplete SCI, the aneurysm clip-compression model was used (Forgione et al., 2014; Iwai et al., 2015; Krupa et al., 2018). Animals were anesthetized by intraperitoneal administration of 1% pentobarbital sodium (25 mg/kg). The dorsal portion of the spinal cord was exposed by a laminectomy at the T9–T11 levels. An aneurysm clip (clamping force: 60–75 g; Sugita, Tokyo, Japan) was used to compress the spinal cord at T10 for 1 minute. The muscle layers and the skin were secured with wound clips. After surgery, rats were injected with penicillin (50,000 unit/kg per day; Macklin, Shanghai, China) intramuscularly for 3 days. Manual micturition and nursing care were applied twice daily to prevent associated complications. hUC-MSCs transplantation was performed at day 7 post SCI. Injured animals were randomly divided into four groups: PBS (n = 12), low dose (0.25×10^6 cells/kg, n = 12), medium dose (1×10^6 cells/kg, n = 12), and high dose (4×10^6 cells/kg, n = 12). Intrathecal administration of 40 µL of either PBS or hUC-MSCs (P3–P6) suspension was performed at the L6 level using a micro-injection pump (R404, RWD, PRC) at the rate of 6 µL/minute. To prevent leakage of transplanted cells, the injection needle was kept within the subarachnoid space for another 2 minutes after transplantation. Cyclosporin A (10 mg/kg, Aladdin, Shanghai, China) was given daily via subcutaneous injection until the end of the experiment. In this study, all rodents were regularly examined for 30 days after intrathecal transplantation.

Behavioral evaluation after hUC-MSC transplantation

Functional recovery was evaluated by a set of behavioral tests, including Basso, Beattie, and Bresnahan (BBB) scoring, beam walk, and Rivlin test. For all three measurements, we carried out three biological replications for all groups and each group started with 12 animals.

BBB scoring

Hindlimb locomotor function was evaluated based on the BBB open-field rating scale (Davies et al., 2017). The BBB rating scale ranges from 0 to 21. A score of 0 means complete posterior paresis, while a score of 21 indicates that the hind legs have completely normal movement and function. Before and every 5 days after intrathecal transplantation, animals were allowed to walk freely for at least 5 minutes prior to examination by two independent observers of hindlimb locomotor frequency, joint movement range, and coordination of motion. In this study, the final BBB score was the mean value of the recorded scores for both hindlimbs.

Beam walk test

Advanced locomotor skills and coordination of hindlimb movement were also measured using a 0–7 point scale in a beam walk test (Dolan and Tator, 1979). A score of 0 means complete posterior paresis, while a score of 7 indicates that the hind legs have complete locomotor skills and coordination of hindlimb movement. Rats were placed on one side of the beam, and an escape box was placed on the other side. The latency and the trajectory to traverse the beam were recorded by a video tracking system (TSE-Systems Inc., Bad Homburg, Germany) for a maximum of 60 seconds. Performance of locomotor coordination was evaluated three times at each time point and the average score was calculated and recorded before and every 5 days after subarachnoid transplantation.

Rivlin test

To quantify motor function recovery in rats, the Rivlin test was carried out according to a previous study (Rivlin and Tator, 1978). A larger angle means a better motor function recovery. Briefly, the rats were placed on a rubber mat of a movable inclined plate with protractors on both sides to measure the slope angle. Rats were trained before the experiment to maintain their position on the inclined plane, which was increased or decreased at 5° intervals, without falling. The maximum tilt angle at which the rat could maintain its position for at least 5 seconds was recorded. Each animal was tested three times at each time point and the average inclination angle was calculated and recorded before and every 5 days after subarachnoid transplantation.

Radiological evaluation

Magnetic resonance imaging (MRI) and diffusion tensor imaging (DTI) were performed to evaluate local inflammation within the lesion site and regeneration of tracking fibers using the Discovery 750 system

(3.0 Tesla, GE Medical Systems, Waukesha, WI, USA). Rats from the different treatment groups were imaged before and at 30 days after intrathecal transplantation (n = 3/group). Rats euthanatized with an intraperitoneal administration of 1% pentobarbital sodium (50 mg/kg) were fastened to the center of the small-animal special coil (Wankang, Jiangyin, Jiangsu, China) and placed on the scanning bed. T2-weighted and DTI images of the SCI site (T7–T12) were then obtained. The parameters for the T2-weighted scans were time of repetition = 3000 ms, matrix = 192 × 192, field of view (FOV) = 100 mm, thickness = 1 mm, spacing = 0 mm, and number of excitations = 8. The parameters for the DTI scans were time of echo = 66.6 ms, time of repetition = 3200 ms, bandwidth = 166.7 kHz, matrix = 96 × 48, FOV = 80 mm, phase FOV = 0.5, thickness = 2 mm, spacing = 0 mm, number of excitations = 10, b (dispersion sensitivity) = 800, and the number of diffusion directions = 9. Image post-processing software (Functool) in the AW 4.6 workstation (GE Healthcare, Chicago, IL, USA) was used to reconstruct MRI T2-weighted and DTI images in both anterior-posterior and sagittal views.

Histology and immunohistochemistry

Immunofluorescence staining was conducted to assess histological repair of injured spinal cords in rats. Six animals in each group were randomly selected and euthanized 30 days after intrathecal transplantation. Following cardiac perfusion with 0.9% sodium chloride containing heparin, anesthetized animals were infused with fixative (PBS containing 4% paraformaldehyde [PFA]). Spinal cord segments of 1.5 cm centered at the lesion epicenter were dissected, fixed in 4% PFA overnight, dehydrated in 30% sucrose solution, and then cut into 20 μm serial coronal sections. Sections were incubated with blocking solution (0.1% Triton X-100 and 10% normal goat serum in PBS) at room temperature for 1 hour, and then stained with primary antibodies against glial fibrillary acidic protein (GFAP, 1:500; Cat# M0761; Dako, Grosschup, Denmark), myelin basic protein (MBP, 1:500; Cat# 10458-1-AP; Proteintech, Wuhan, Hubei, China), and microtubule-associated protein 2 (MAP2, 1:100; Cat# sc-74421; Santa Cruz Biotechnology, Santa Cruz, CA, USA) overnight at 4°C, followed by secondary antibody goat-anti-chicken IgG H&L (Alexa Fluor® 568, 1:2000; Cat# ab175711; Abcam, Cambridge, UK) or goat-anti-rabbit IgG H&L (Alexa Fluor® 488, 1:2000; Cat# ab150077; Abcam) for 1 hour at room temperature. Cell nuclei were counterstained with 1 g/mL 4′,6-diamidino-2-phenylindole (DAPI; MilliporeSigma) for 15 minutes.

Hematoxylin and eosin (H&E) staining was applied to sections to measure the cavity size. Briefly, spinal cord sections were stained with hematoxylin and washed twice with distilled water before differentiation with 1% hydrochloric acid to remove the non-specific background staining. Subsequently, the eosin counterstain was performed. Sections were photographed using an optical upright microscope (LSM 880 with Airyscan; Zeiss, Jena, Germany). The immunofluorescent intensity of certain antibody and H&E-stained areas in the brightfield microscopy images were quantified using the ImageJ software (version 1.8.0, NIH, Bethesda, MD, USA) (Schneider et al., 2012). Overall, three tissue samples per group were evaluated to calculate group means for statistical comparisons.

Western blotting

To evaluate SCI repair by protein expression level, western blot analysis was performed. Spinal cord segments spanning 1 mm from each side of the lesion were quickly dissected for protein extraction 30 days after intrathecal transplantation (n = 3 per group). The samples were homogenized on ice in radioimmunoprecipitation assay buffer (RIPA; 150 mM NaCl, 50 mM Tris-HCl, pH 8.0, 5 mM EDTA, 1% Triton X-100, 0.1% SDS, 1% sodium deoxycholate, 1 mM PMSF, 10 mg/mL aprotinin, 5 mg/mL leupeptin). The lysates were centrifuged at 12 × g for 10 minutes at 4°C. The proteins in the supernatant were separated by SDS-PAGE and transferred to a nitrocellulose filter membrane (Hybond-P, Amersham Pharmacia Biotech, Buckinghamshire, UK). The membrane was blocked in Tris-buffered saline with 0.1% Tween-20 (TBST) with 5% fat-free milk for 1 hour, and then incubated with the primary antibodies overnight at 4°C. The primary antibodies used were: rabbit anti-GFAP (1:3000; Cat# M0761; Dako, Grosschup, Denmark), rabbit anti-MBP (1:3000; Cat# 10458-1-AP; Proteintech), mouse anti-MAP2 (1:5000; Cat# sc-74421; Santa Cruz Biotechnology), and mouse GAPDH monoclonal antibody (1:5000; Cat# RM2002; Beijing Ray Antibody Biotech, Beijing, China). After three washes with TBST, the membranes were incubated for 1 hour at room temperature with the secondary peroxidase-conjugated antibodies peroxidase AffiniPure goat anti-rabbit IgG (H+L) (1:3000; Cat# 111-035-003; Jackson, PA, USA) or peroxidase AffiniPure goat anti-mouse IgG (H+L) (1:3000; Cat# 115-035-003; Jackson), which were diluted in TBST containing 5% fat-free milk. The chemiluminescence-based immunodetection system (ECL, Invitrogen, Carlsbad, CA, USA) of horse radish peroxidase (HRP) was used and the membranes were exposed to X-rays. The relative expression levels of proteins were quantified using the ImageJ software (Version 1.8.0). Three independent experiments were conducted.

Biotinylated dextran amine tracing of the rat corticospinal tract

The axonal regrowth was traced by an extracellular injection of biotinylated dextran amine (BDA) 2 weeks before the termination of the experiments as described previously (Han et al., 2020). Briefly, four animals per group were used for BDA injection to ensure at least three survivals at the end of the experiment. A window (10 mm long and 5 mm wide) was made by a microdrill in the posterior skull 0.5 mm posterior to the coronal suture to expose the sensorimotor cortex. The coordinates at the X, Y, and Z axes determine the medial-to-lateral, the anterior-to-posterior, and the dorsal-to-ventral distance from the bregma, respectively. Twenty-four microinjections (0.25 μL per injection) of BDA (10,000 MW, 10% in PBS; Thermo Fisher Scientific, Waltham, MA, USA) were delivered into brain regions at a rate of 50 nL/minute by a 5 μL Hamilton syringe targeting the corticospinal tract in the brain to study axon regeneration in the SCI area, with the following coordinates: mediolateral coordinates (x-axis): –2.5, –1.25, 1.25, and 2.5 mm; anteroposterior coordinates (y-axis): –1.0, –2.5, and –4.0 mm; dorsoventral coordinates (z-axis): –0.5 and –1.0 mm. The needle was left in place for another 2 minutes after each injection. To visualize the BDA^+ axons, spinal cord sections were incubated with Alexa Fluor 568 conjugated-streptavidin (1:1000, Thermo Fisher Scientific) and images were captured by an optical upright microscope. Because the size of the injured spinal cord was larger than the microscope field of view, we collected multiple images per slice using a 2.5× objective. Manual stitching of multiple fields in a single mosaic image was performed.

Electrophysiological measurements

To monitor functional changes in descending pathways between the motion cortex and motor neurons, cortical motor evoked potential (MEP) signals in the left hindlimb were acquired before and 30 days after hUC-MSC transplantation using the BL-420 A/F Data Acquisition Analysis System (TAIMENG SOFTWARE, Chengdu, China). Seven animals from each group were examined. In brief, after rats were anesthetized by intraperitoneal administration of 1% pentobarbital sodium (25 mg/kg), their motor cortices were exposed in a stereotaxic apparatus (Joshi and Fehlings, 2002). Stimulating electrodes were placed in the representative hindlimb area of the right motor cortex, which included a positive needle electrode and a negative needle electrode. The recording electrode was inserted into the gastrocnemius muscle of the contralateral hindlimb. The earthing line was positioned between the stimulating and recording electrodes. The electrical stimulation parameters were 10 V, 1 millisecond pulse width, 50 ms, and 10 Hz frequency, and then the amplitude (mV) and latency (ms) of the MEPs were acquired.

Reverse transcription and real-time PCR

Spinal cord samples containing the lesion epicenter with a length of approximately 5 mm were dissected from each group 30 days post transplantation (n = 6 per group). Reverse transcription and real-time PCR were performed as previously described (Li et al., 2012). Briefly, total RNA was purified with Trizol reagent (Takara, Shiga, Japan). A reverse transcription system (ABI, New York, NY, USA) was applied to convert 1 μg of total RNA into cDNA. Real-time PCR was performed in triplicates using SYBR Green PCR Master Mix (YEASEN, Shanghai, China) and the ABI-StepOnePlus™ system (Thermo Fisher Scientific). The reaction program was as follows: initial denaturation at 95°C for 30 seconds, followed by 50 cycles of denaturation at 95°C for 10 seconds and annealing at 60°C for 30 seconds. The internal control was 28S rRNA. The relative expression ratio of the target mRNA was normalized to the GAPDH gene expression using the ΔCt method ($2^{-\Delta\Delta Ct}$).

Statistical analysis

No statistical methods were used to predetermine sample sizes; however, our sample sizes are similar to those reported in a previous publication (Yang et al., 2020b). Biochemical, histological, and behavioral analyses were conducted blinded to treatment, whereas *in vivo* microscopy and analysis were not performed blinded to

the conditions of the experiments. Data are presented as mean ± standard error of the mean (SEM). One-way or two-way analysis of variance (ANOVA) was performed using SPSS software (Version 17.0, SPSS, Chicago, IL, USA) and statistical significance was defined as $P < 0.05$.

Results

Both the medium and high doses of hUC-MSCs lead to functional recovery in rats with subacute SCI

To search for a more accurate dose range for clinical translation, we first compared the therapeutic effects of three different hUC-MSC doses: low dose (0.25×10^6 hUC-MSCs/kg), medium dose (1×10^6 hUC-MSCs/kg), and high dose (4×10^6 hUC-MSCs/kg), on the recovery of hindlimb locomotion after subacute SCI. We documented movement patterns displayed by rats from different groups during the entire investigation period (**Figure 1A** and **B**). Compared with the intact rats, which moved voluntarily, bearing their full weight on their hind legs, the paralyzed rats in the subacute phase of SCI stood up with the dorsal surface of the hind paws contacting the ground and moved forward in a manner depended on the forelimb steps. At 30 days after transplantation, rats treated with PBS or low-dose hUC-MSCs showed limited and spontaneous functional improvement without complete touching of the ground with the soles of the hind paws. By contrast, rats that received the medium or high doses exhibited persistent locomotion recovery and could stand up with plantar placement of the hind paws. Behavioral analyses, including the BBB score (**Figure 1C**), beam walk test (**Figure 1D**), and Rivlin test (**Figure 1E**), were performed and scores were obtained every 5 days. The results were similar for all three measurements. One week after SCI and right before transplantation, all animals, which were randomly grouped, showed no significant differences in BBB score (1.52 ± 0.13), beam walk score (1), and Rivlin score (28.96 ± 0.38). The low dose group failed to improve in locomotor function compared with the PBS group during the entire investigation period, reaching a maximum BBB score of 3.75 ± 0.21. In contrast, significant improvement in the BBB score was observed in both the medium and high dose groups as early as 15 days ($P < 0.001$) and 5 days ($P < 0.05$) post transplantation, respectively. These animals exhibited increased functional improvement in the BBB score with 7.5 ± 0.37 for the medium dose group and 8.16 ± 0.20 for the high dose group until the end of this study, indicating extensive movement of all three joints of the hindlimbs and even plantar stepping with occasional weight bearing. No significant difference between the medium and high dose groups was observed. Regarding the beam walk test, no statistical significance was observed between the PBS control and low dose groups 30 days after transplantation, which was consistent with the BBB scores. The best scores were obtained by both the medium and high dose groups (3.66 ± 0.14) with no statistically significant difference. The Rivlin test was performed to evaluate the coordination of the hind limbs. The earliest improvement was observed in the medium dose group 10 days after treatment ($P < 0.001$). A similar recovery trend was observed in the high does group (**Figure 1E**). Taken together, rats in the PBS and low dose groups showed no significant improvements in these three behavioral indicators compared with pre-transplantation, whereas animals in the medium and high dose groups demonstrated statistically significant improvement. These results suggest that the medium and high dose-injected rats recovered significantly better than rats in the PBS and low dose groups, indicating that both the medium and high doses were effective in SCI treatment, whereas the low dose was not.

Both the medium and high doses of hUC-MSCs considerably increase tissue sparing at the injury site

The gross morphology of the spinal cord of all experimental groups at the C5–L5 level exhibited loss of tissue at the lesion site compared with the intact group with better preservation observed in the medium and high dose groups (**Figure 2A**). Furthermore, the integrity of the spinal parenchyma determined by H&E staining of sagittal sections of spinal cords containing the lesion epicenter supported the finding that the two effective doses significantly improved anatomical outcomes by showing better connections and reduced cavity area compared with the PBS and low dose groups (**Figure 2B**). Quantification of the lesion size revealed that the effective doses elicited a three-fold decrease in the cyst size compared with that in the PBS and low dose groups (**Figure 2B**, lower panel). To measure the hUC-MSC-mediated recovery by a less invasive method, we used MRI and DTI, which are ideal outcome measures for human SCI clinical studies. A high-intensity zone in T2-weighted MRI images confirmed the presence of edema and necrosis within the injured site in all four groups at the subacute SCI stage. At 30 days after intrathecal transplantation, the decreased signal intensity in both the medium and high dose groups showed a mild improvement in the damaged area compared with that in the PBS and low dose groups (**Figure 2C**). The DTI tractography was used to track the damage and recovery of nerve fibers. We found that in intact spinal cords, the fiber signals were well organized and filled the entire spinal cord (**Figure 2D**, left panel), while the subacute SCI caused a nearly complete disruption of nerve fibers in all groups before transplantation **(Figure 2D**, right upper panels). As expected, the gap persisted in the PBS and low dose groups, whereas the medium and high dose of hUC-MSC treatments induced regeneration of fiber tracts, thereby reconnecting the rostral and caudal ends of the injured cord (**Figure 2D**, right lower panels).

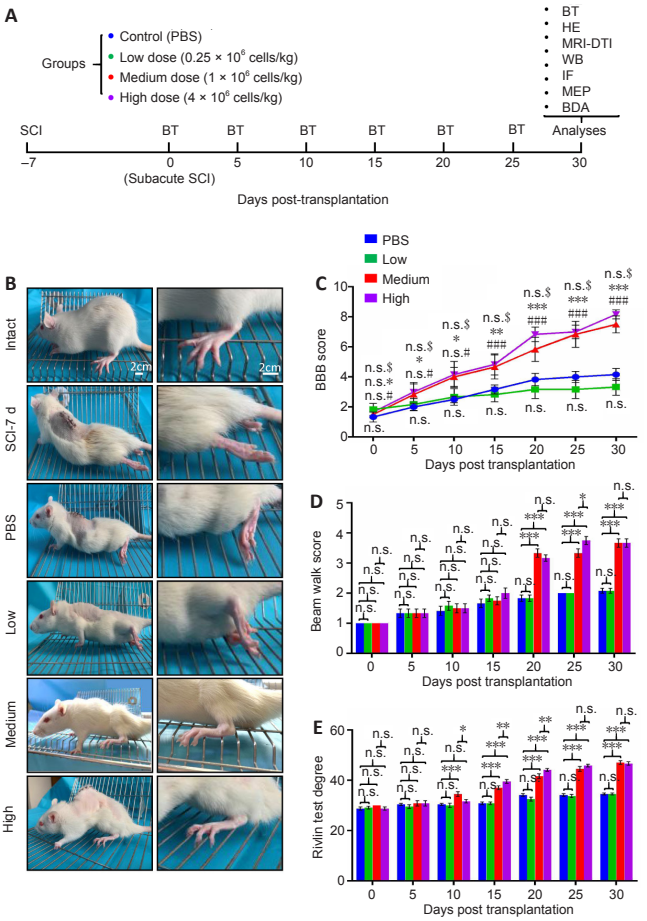

Figure 1 | Both the medium and high doses of hUC-MSCs exhibit functional recovery post subacute SCI.

(A) Experimental scheme. Rats at the subacute SCI stage were randomly divided into four groups that received PBS or human umbilical cord mesenchymal stem cells (hUC-MSCs) at different doses. The behavioral tests were performed every 5 days and combinational efficacy analyses were carried out 30 days post implantation. BDA: Biotinylated dextran amine; BT: behavioral test; DTI: diffusion tensor imaging; HE: H & E staining; IF: immunofluorescence; MEP: motor evoked potential; MRI: magnetic resonance imaging; RT-QPCR: reverse transcription quantitative real-time PCR; WB: western blotting. (B) Representative images of rats with different treatments 5 weeks after injury. Intact: Normal rat; SCI-7d: subacute SCI; PBS: phosphate-buffered saline; Low: low dose (0.25×10^6 cells/kg); Medium: medium dose (1×10^6 cells/kg); High: high dose (4×10^6 cells/kg). (C–E) A series of behavioral tests to evaluate the dose effect of hUC-MSCs on locomotor functions using the BBB score (C), beam walk score (D), and Rivlin score (E). Data are presented as mean ± SEM; $n = 9$/group. n.s.: Not significant between PBS and low dose; #$P < 0.05$, ###$P < 0.001$ between PBS and medium dose; *$P < 0.05$, **$P < 0.01$, ***$P < 0.001$ between PBS and high dose; n.s.$: not significant between medium and high dose by two-way analysis of variance.

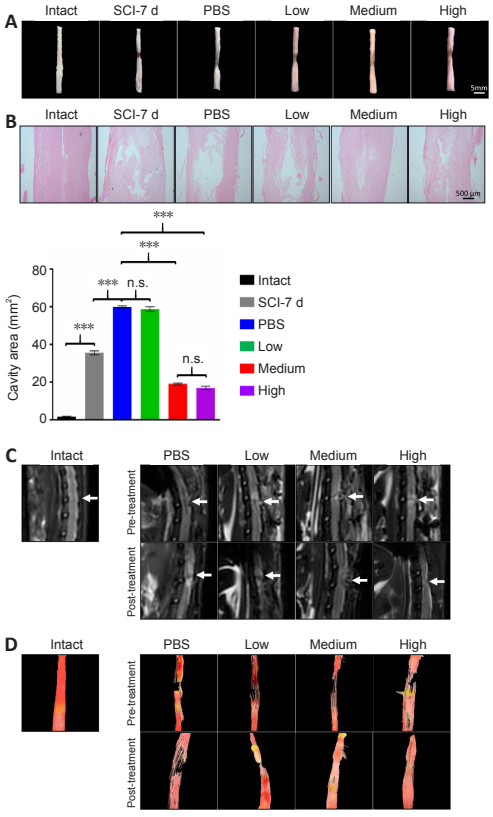

Figure 2 | **Both the medium and high doses of human umbilical cord mesenchymal stem cells considerably enhance spinal cord tissue retention 30 days post implantation.**

(A, B) Representative images of the gross morphology of spinal cords at the C5–L5 levels (A) and hematoxylin and eosin (H&E) staining of spinal cords at the lesion sites (B) 4-weeks post transplantation. The medium and high dose groups demonstrated significantly improved anatomical outcomes compared with the PBS and low dose groups. Lower panel in B: quantification of the lesion area. Data are presented as the mean ± SEM; n = 3/group. n.s.: Not significant; ***P < 0.001 (one-way analysis of variance). (C) Representative T2-weighted MRI images of a spinal cord in each group. White arrows indicate the surgical site. Both the medium and high dose groups showed decreased signal intensity in the damaged area compared with the PBS and low dose groups. (D) Representative diffusion tensor images of a spinal cord from rats in different groups. The medium and high dose of MSC treatments induced regeneration of fiber tracts. Pre-transplantation in C and D: subacute phase (7 days after injury); post transplantation in C and D: 30 days post implantation. Intact: Normal rat; SCI-7d: subacute SCI; PBS: phosphate-buffered saline; Low: low dose (0.25×10^6 cells/kg); Medium: medium dose (1×10^6 cells/kg); High: high dose (4×10^6 cells/kg).

Both the medium and high doses of hUC-MSCs reduce astrocytic scarring and enhance neuronal growth and remyelination

To evaluate the extent of host cellular responses after hUC-MSCs transplantation, we compared the expression of the markers for glial scar formation, neurogenesis, and axonal remyelination, namely GFAP, MAP2, and MBP, respectively, at the mRNA and protein levels among all groups (**Figure 3**). The dramatically increased GFAP mRNA level caused by the SCI in the PBS group was significantly inhibited by both the effective doses but not by the low dose at 30 days post transplantation (**Figure 3A**; left panel). Moreover, the high dose inhibited the level of *GFAP* slightly more than the medium dose. Additionally, the transcriptional repression of *MAP2* and *MBP* induced by the SCI was significantly reversed by approximately the same extent by both effective doses (P < 0.01 for MAP2, P < 0.001 for MBP) with no significant difference between them (**Figure 3A**; middle and right panels). In contrast, the low dose did not improve the decrease in mRNA levels of these two genes. The protein levels of these three genes evaluated by western blotting were consistent with the mRNA levels, and the medium and high doses induced the same extent of recovery (**Figure 3B** and **C**). To visualize the distribution and intensity of proteins at the lesion site, immunofluorescence staining was applied to all groups. Glial scar formation is generally defined by recruitment of reactive astrocytes, which highly express GFAP, to the lesion site. The distances between the lesion edges, which were traced by high intensity of GFAP signals, were longer in the PBS and low dose groups than they were in the medium and high dose groups (**Figure 3D**; upper panels). A significant reduction in the total intensity of GFAP immunoreactivity was observed in both the medium and high dose groups, in contrast to the PBS and low dose groups. Furthermore, there were more scattered astrocytes bridging the lesion gap in the medium and high dose groups, which is consistent with the results obtained by the He group, suggesting that $GFAP^+$ astrocytes play an important role in allowing axons to grow across the lesion (Zukor et al., 2013). In contrast to the GFAP immunoreactivity, the quantification of MAP2, the neuron-specific cytoskeletal protein enriched in the soma and dendrites, revealed a significant increase in the total intensity in both effective dose groups (**Figure 3E** and **G**). Again, we did not observe a difference in the intensity of MAP2 staining between the restoration in the low dose group and the spontaneous recovery in the PBS control. The demyelination following the SCI and the remyelination that occurred after hUC-MSC transplantation was easily identified by the increase in the MBP-positive area in both the medium and high dose groups, compared with the other two groups (**Figure 3F** and **G**). Overall, these results suggest that both the medium and high doses of hUC-MSCs alleviated fibrotic scar formation and increased neuronal growth and remyelination. Of note, GFP-labeled hUC-MSCs were used to examine the distribution of transplanted cells adjacent to and within the lesion epicenter at 4-weeks post graft and no consistently detectable signals were obtained (data not shown), which is consistent with our previous study showing that a handful of transplanted hUC-MSCs remained alive and differentiated in the spinal cord (Yang et al., 2020b). Therefore, the improved spinal integrity mediated by hUC-MSCs after subacute SCI was not mainly because of direct integration and differentiation of engrafted cells, if any, across the injury stie.

Both the medium and high doses of hUC-MSCs promote axonal regrowth

The regeneration of the corticospinal projections is important for enhancing voluntary motor movement after SCI. To evaluate whether both the effective doses can activate the growth of axons in injured spinal cord, we injected the axon tracer BDA into the sensorimotor cortex (**Figure 4A**) and quantified BDA-labeled corticospinal tract (CST) axons at different distances from the lesion site (**Figure 4H**). Coronal sections of the lesion were also stained for GFAP to mark the lesion edges. Because the rat model that we used in this study was subjected to incomplete SCI, we defined BDA-labeled axons projecting into and through the lesion site as axonal regrowth, which may include axonal regeneration and/or sprouting. The immunofluorescence staining showed that nearly all nerve fibers were well aligned in the intact group (**Figure 4B**). The gap between the GFAP-stained zone/barrier was shortened in the medium and high dose treatments compared with the PBS and low dose groups (**Figure 4D–G**), which is consistent with our previous observations (**Figure 3D**). In the PBS control and low dose groups, although many organized BDA-labeled nerve fibers were observed far rostral to the compression injury site (**Figure 4D-a** and **E-a**), there were small numbers of these axons immediately rostral to the lesion cavity (**Figure 4D-b** and **E-b**) and almost no signals were detected in the center of (**Figure 4D-c** and **E-c**) and caudal to the lesion cavity (**Figure 4D-d**, **D-e**, **E-d**, and **E-e**). Nevertheless, several BDA-labeled axons bypassed the lesion site in both the medium and high dose-treated rats (**Figure 4F** and **G**). Furthermore, in the medium and high dose-treated rats, there were several irregular and scattered BDA-positive axons that entered the cyst (**Figure 4F-c** and **G-c**), and occasional BDA-positive fibers located immediately caudal to the lesion (**Figure 4F-d** and **G-d**) and even ~7 mm distal to the caudal lesion edge (**Figure 4F-e** and **G-e**), which is indicative of long-distance axonal regrowth to regenerate a neural circuit relay through the lesion area. Quantification and comparison of the BDA fluorescence intensity at different distances from the epicenter in all groups revealed significant effects of both the effective dose groups (P < 0.001) on axonal regrowth (**Figure 4H**). Additionally, we noticed several co-localization signals between the CST axons and astrocytes across the lesion in both the effective dose groups, which is consistent with previous observations (Zukor et al., 2013), suggesting that astrocytes play important roles in promoting regeneration of CST axons after SCI. Moreover, the anterograde axonal tract tracing revealed that the medium and high doses of hUC-MSCs promoted axonal regrowth through the injury site to form a new neuronal relay circuit.

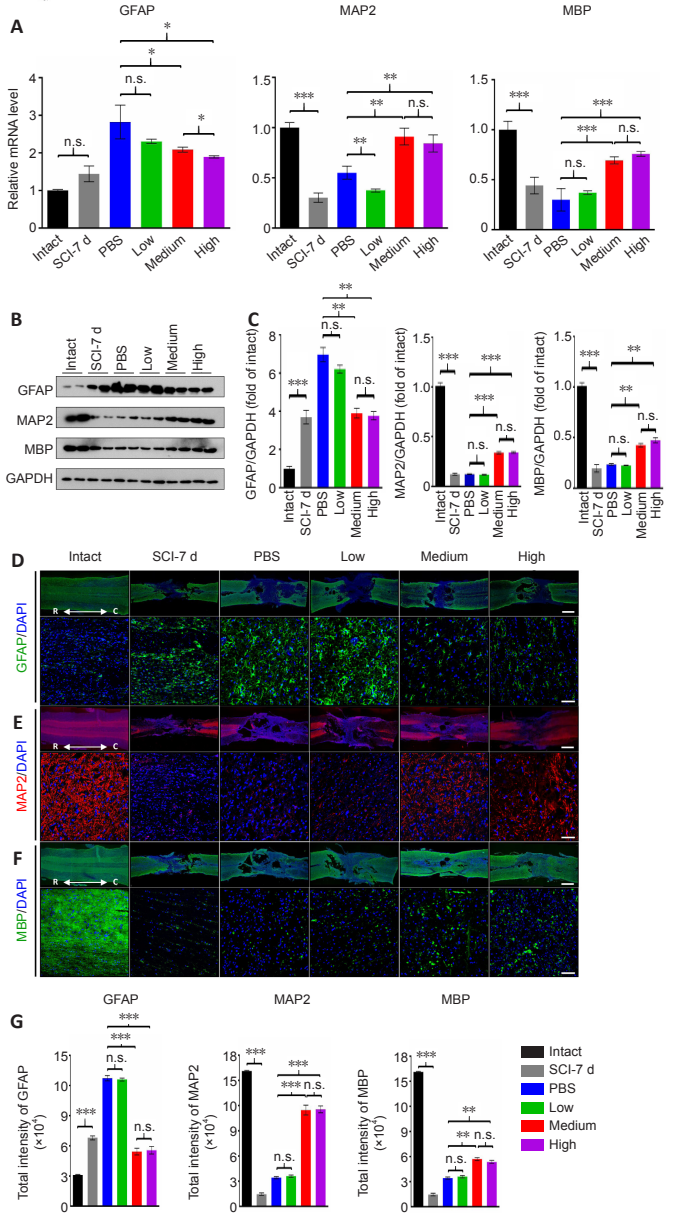

Figure 3 | **Both the medium and high doses of human umbilical cord mesenchymal stem cells lead to reduced astrocytic scarring and enhanced axonal regrowth and remyelination at 4 weeks after transplantation.**
(A) Real-time PCR to measure the mRNA levels of GFAP, MAP2 and MBP in all groups, respectively. (B) Western blot analysis of GFAP, MAP2 and MBP in all groups, respectively. Glyceraldehyde-3-phosphate dehydrogenase (GAPDH) was used as loading control. (C) Quantification and comparison of protein markers in all groups. The histograms show the densitometric analysis. (D–F) Representative immunofluorescence images of coronal sections of the lesion stained for GFAP (D), MAP2 (E), and MBP (F) in all groups. Upper panels: low magnification images. Lower panels: high magnification of area immediately close to the lesion site. Scale bars: 500 μm in the upper panels; 100 μm in the lower panels. C: Caudal; R: rostral. (G) Quantification of immunofluorescence intensities in the high magnification images of all groups in D–F. Intact: Normal rat; SCI-7d: subacute SCI; PBS: phosphate-buffered saline; Low: low dose (0.25×10^6 cells/kg); Medium: medium dose (1×10^6 cells/kg); High: high dose (4×10^6 cells/kg). For all panels, data are presented as the mean ± SEM; $n \geq 3$/group; n.s.: not significant; $^*P < 0.05$, $^{**}P < 0.01$, $^{***}P < 0.001$ (one-way analysis of variance).

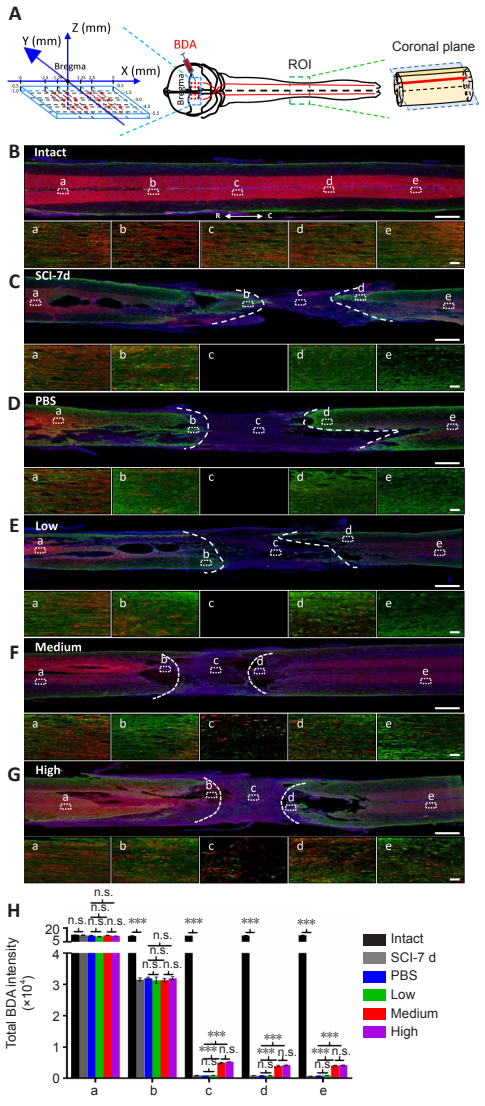

Figure 4 | **Both the medium and high doses of human umbilical cord mesenchymal stem cells promote axonal regrowth after subacute SCI.**
(A) Schematic diagram illustrating the experimental design of the corticospinal tract (CST) anterograde tracing using bilateral biotinylated dextran amine (BDA) injection into the sensorimotor cortex. Left panel: the coordinates of 24 BDA injection sites (red dots). Right panel: illustration showing the BDA-labeled CST in a spinal cord segment. The blue dotted rectangle indicates the coronal plane through the BDA-labeled CST main tract. ROI: region of interest. (B–G) BDA-labeled axons in coronal sections of the injured spinal cord coimmunostained with GFAP (green) and DAPI (blue) in intact (B), subacute SCI (7 days post SCI) (C), PBS control (D), low dose (E), medium dose (F), and high dose (G) groups 4-weeks post transplantation. Lower panels in B–G: high magnification of the dotted rectangular areas in the upper panel showing different views located far rostral to (a), immediately rostral to (b), in the middle of (c), immediately caudal to (d), and far caudal to (e) the lesion site. White dashed lines represent the edges of the injury site identified by GFAP. Scale bars: 1 mm in B–G and 50 μm in a–e. (H) Quantification and comparison of BDA total intensities in B–G. Intact: Normal rat; SCI-7d: subacute SCI; PBS: phosphate-buffered saline; Low: low dose (0.25×10^6 cells/kg); Medium: medium dose (1×10^6 cells/kg); High: high dose (4×10^6 cells/kg). For all panels, data are presented as mean ± SEM; $n \geq 3$/group; n.s.: not significant; $^{***}P < 0.001$ (one-way analysis of variance).

Both the medium and high doses of hUC-MSCs improve the functional integrity of the descending motor pathways in the spinal cord

To further assess the functional integrity of spinal pathways, MEPs were recorded right before and 4 weeks after transplantation (**Figure 5**). A single stimulation was applied to the right motor cortex and the excitability of the CST was measured in contralateral hindlimb muscles (**Figure 5A**). The MEPs at the subacute-SCI stage among all groups were barely detected before cell transplantation. Following the intrathecal infusion of hUC-MSCs, only a very weak signal above background was recorded from the PBS (0.14 ± 0.02 mV) and low dose (0.14 ± 0.02 mV) groups, whereas a significantly increased amplitude was observed in both the medium (0.71 ± 0.02 mV) and high dose (0.72 ± 0.03 mV) groups (**Figure 5B** and **C**), suggesting a dose-dependent recovery of connections in the spinal cord. Furthermore, the latency was significantly delayed in the subacute phase of the SCI (11.51 ± 0.13 ms) compared with that in the intact group (6.45 ± 0.17 ms; $P < 0.001$), and the medium (8.78 ± 0.18 ms) and high dose (8.65 ± 0.21 ms) treatments shortened the latency of the stimulation response compared with that in the PBS (12.54 ± 0.45

ms) and low dose (12.4 ± 0.57 ms) groups at 4 weeks post treatment (**Figure 5B** and **D**). There was no significant difference in the MEPs between the medium and high dose groups, which further supports the comparable effects of both these doses. Taken together, these data suggest that the cortical-spinal connection through the injured spinal cord can be reestablished by the medium and high hUC-MSC doses.

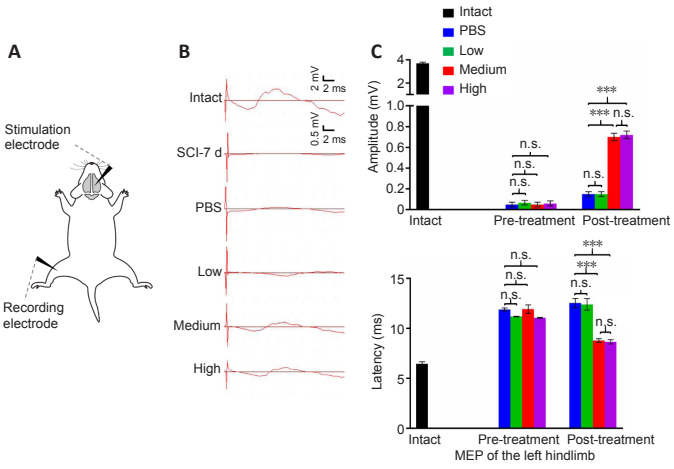

Figure 5 | **Both the medium and high dose treatments facilitate the transmission of descending inputs from the brain.**
(A) Schematic diagrams of the motor evoked potential (MEP) assessments. Black arrowheads represent the stimulation and recording electrode. (B) Representative MEP recordings in rats with different treatments after SCI. Quantification and statistical analyses of amplitude (C) and latency period (D) of MEPs are shown. Intact: Normal rat; SCI-7d: subacute SCI; PBS: phosphate-buffered saline; Low: low dose (0.25×10^6 cells/kg); Medium: medium dose (1×10^6 cells/kg); High: high dose (4×10^6 cells/kg). Data are presented as the mean ± SEM; n = 7/group; n.s.: not significant, ***$P < 0.001$ (one-way analysis of variance).

Both the medium and high doses of hUC-MSCs partially restore the decreased transcription levels of ion channels and neurotransmitter receptors at the lesion site after subacute SCI

To accurately maintain descending commands from the brain, the gene expression levels of ion channels and neurotransmitter receptors in the spinal cord must be properly orchestrated to shape their electrophysiological activity. Because both the medium and high doses of hUC-MSC injection led to significant locomotor recovery, especially the improved electrophysiological outcome, we hypothesized that the effective doses of hUC-MSCs may function through a molecular mechanism that restors the expression of ion channels and receptors in the spinal cord. To test this, we compared the mRNA levels of 40 genes coding for the protein subunits that constitute the calcium channels (*Cacna1a*, *Cacna1b*, *Cacna1e*, *Cacna2d1*, *Cacna2d2*, *Cacna2d3*, *Cacna1i*, *Cacnb2*, *Cacng2*), potassium channels (*Kcna1*, *Kcna2*, *Kcna3*, *Kcnab1*, *Kcnab2*, *Kcnc1*, *Kcnc2*, *Kcnc3*, *Kcnk9*, *Kcnq2*), cholinergic receptor (*Chrna2*, *Chrnb2* and *Chrm2*), glutamate metabotropic receptor (*Grm1*, *Grm2*, *Grm3*, *Grm4*), 5-hydroxytryptamine receptor (*Htr1a*, *Htr1b*, *Htr2a*, *Htr2c*), dopamine receptor (*Drd2*, *Drd5*), glycine receptor (Glra1, Glra2 and *Glra3*), and γ-aminobutyric acid (GABA) type A ($GABA_A$) receptor and related genes (*Gabra1*, *Gabra3*, *Gabrb3*, *Gabrg2* as well as potassium-chloride cotransporter 2 [KCC2] and GABA vesicular transporter Slc32a1) in the lesion area among all groups (**Figure 6**). The injury triggered the downregulation of the vast majority of the genes we monitored at the subacute SCI phase and the decreased transcription levels were even lower in the PBS control group at 4-weeks post SCI. The low dose treatment increased the expression of some transcripts belonging to the ion channels and receptors with the exception of all $GABA_A$ receptors and GABA vesicular transporter Slc32a1. A significant upregulation of almost all genes, except for *Kcna3* and *Grm2* in the medium dose group, was detected in both the medium and high dose groups compared with the PBS control. The partially reversed expression of the reduced ion channels and neurotransmitter receptors by both the effective doses suggests that intrathecal administration of hUC-MSCs at a density of 1–4 × 10^6/kg may also contribute to the regeneration of neuronal relays after SCI. In particular, the $GABA_A$ receptors, which were only increased by the effective doses, may serve as potential therapeutic targets to improve the reconnection of damaged neuronal circuits.

Discussion

A substantial number of patients worldwide are still suffering from SCI because of the limited treatment options including surgical interventions and rehabilitative care. On the basis of the promising results generated by experimental studies, stem cell therapy is emerging as a cutting-edge tool in the field of regenerative medicine to treat SCI. Among the different types of stem cells, hUC-MSCs are one of the most common sources of MSCs used in clinical trials. However, modest clinical efficacy hampered the progression of the clinical translation of hUC-MSCs. This discrepancy may be due to many variables, such as cell source, timing of implantation, route of administration, and relevant efficacious cell doses, which are critical factors that affect the efficacy of treatment in patients with SCI. To produce more clinically relevant results, more precise criteria should be tested in preclinical studies. Searching for a more accurate dose range for intrathecal transplantation of hUC-MSCs for treating subacute incomplete SCI in the clinic, we obtained more concrete evidence through a comprehensive dose comparison study. We found that 1×10^6 but not 0.25×10^6 hUC-MSCs/kg was as efficient as 4×10^6 hUC-MSCs/kg in producing positive outcomes for SCI repair.

Although several studies have applied various sources of MSCs on different models of SCI (Li et al., 2021), the best dose for certain routes of administration of hUC-MSCs has not been fully elucidated. Regarding the route of administration, although intravenous injection is the most reproducible and least invasive method that has been widely used in numerous preclinical studies of SCI management (Kabat et al., 2020), the efficient delivery of MSCs to the area of injury is attenuated mainly by the pulmonary first-pass effect (Fischer et al., 2009), which may account for the use of very high doses. According to recently reported trials using intravenous injection, the minimal effective doses range from 7×10^7 to 1.9×10^8 MSCs/patient/dose and much higher doses of at least 9×10^8 cells were used in two trials. Recently, Dos Santos Ramalho et al. (2019) have performed a dose-response analysis of intraperitoneal implantation of mouse bone marrow-derived stem cells (BMSCs) in a mouse model of compressive SCI and demonstrated that 8×10^5 BMSCs/dose, equivalent to a dose of 3.2×10^7 cells/kg, was a good choice for SCI treatment, which is much higher than the effective doses that we determined. Intrathecal administration is the second most common route, especially in neurological trials. The median dose used for intrathecal delivery in clinical trials so far is around 1×10^8 MSCs/dose. In this study, we chose to test a relatively limited dose range, from 0.25×10^6 to 4×10^6 cells/kg, because we and our collaborators have reported that 4×10^6 hUC-MSCs/kg is safe and efficient for the treatment of subacute SCI through intrathecal implantation in rat models (Yang et al., 2020b). On the basis of this information, we further narrowed the effective dose down to 6.5×10^7 hUC-MSCs/patient (assuming the average weight of an adult is approximately 65 kg), which is sufficient to produce positive outcomes comparable to 2.6×10^8 cells. Our results indicate that minor changes in cell dose can have significantly different consequences. In accordance with our recent study, three ongoing phase 2 clinical trials (NCT03505034, NCT03521336, and NCT03521323) using the medium dose of hUC-MSCs to evaluate the safety and efficacy of intrathecal hUC-MSC administration for the treatment of subacute, early-stage, and late-stage chronic SCI are being conducted by our collaborators (Yang et al., 2020a, 2021). According to the preliminary results obtained so far, they demonstrated that 4-month intrathecal transplantations of allogeneic hUC-MSCs at a dose of 1×10^6 cells/kg/month are safe and effective to achieve significant improvement of neurological dysfunction and a better quality of life.

The main obstacle in developing effective treatments for SCI is our poor understanding of the pathophysiological, cellular, and molecular mechanisms of SCI owing to the disease complexity. Several studies have been conducted to analyze the spinal cord transcriptome after SCI, which causes widespread changes in gene expression across numerous gene families (Chen et al., 2013, 2015; Duan et al., 2015; Shi et al., 2017; Squair et al., 2018; Zhao et al., 2018). In particular, using weighted gene co-expression network analysis on a series of comprehensive transcriptome datasets of injured spinal cord, Duan and colleagues identified 10 gene modules underlying pathological events post SCI, among which synaptic transmission-related genes, including neurotransmitter receptors,

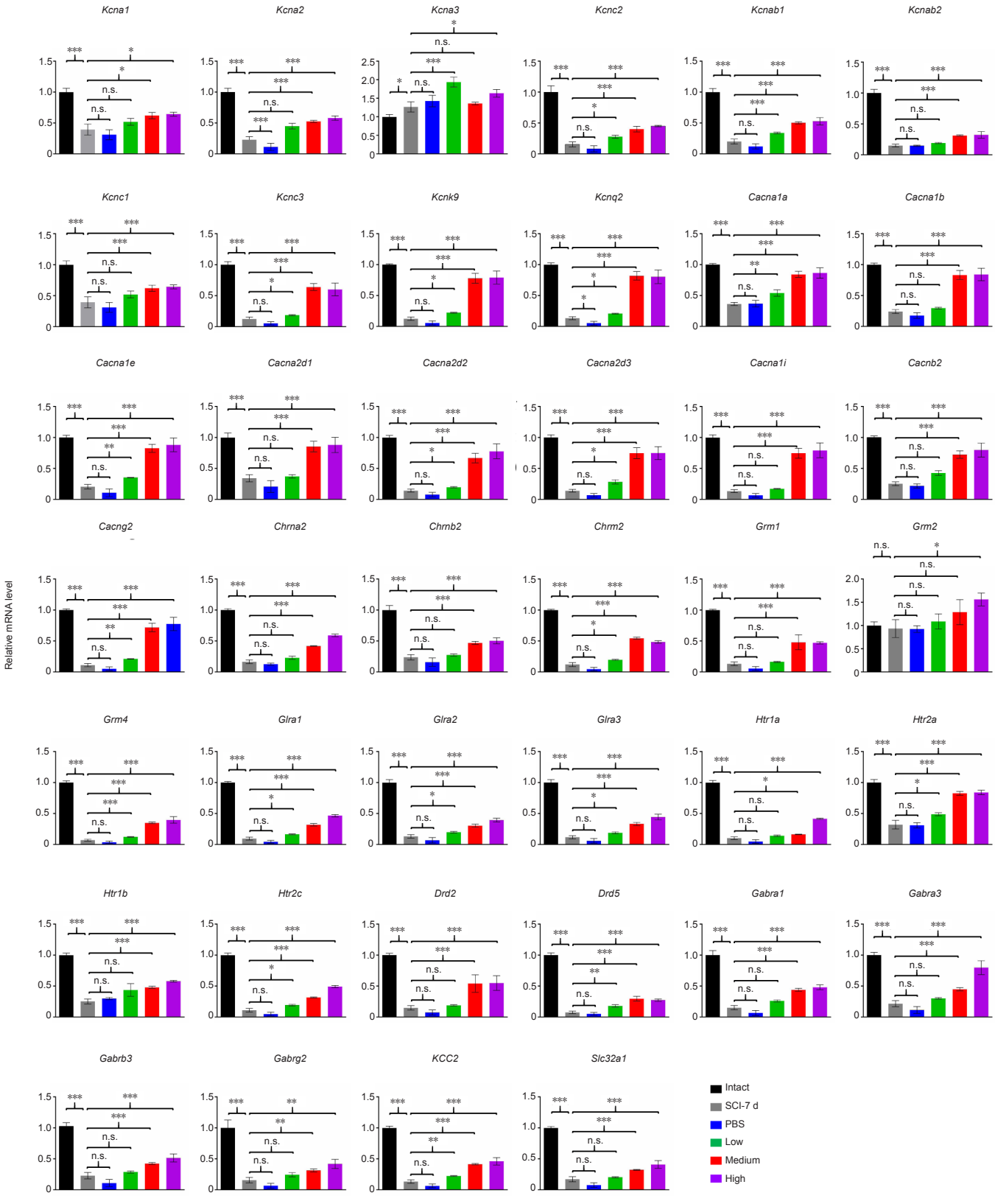

Figure 6 | **Both the medium and high dose treatments partially restore the mRNA levels of genes coding ion channels and neurotransmitter receptors at the lesion site.**

Real-time PCR analysis of the dosage effect of the human umbilical cord mesenchymal stem cell treatment on the repression of 40 ion channels and neurotransmitter receptors. Intact: Normal rat; SCI-7d: subacute SCI; PBS: phosphate-buffered saline; Low: low dose (0.25×10^6 cells/kg); Medium: medium dose (1×10^6 cells/kg); High: high dose (4×10^6 cells/kg). Data are presented as mean ± SEM; $n \geq 3$/group; n.s.: not significant; $^*P < 0.05$, $^{**}P < 0.01$, $^{***}P < 0.001$ (one-way analysis of variance).

ion channels, and axon/dendrite-related genes, underwent dramatic downregulation immediately and remained low after SCI, indicative of long-term impairment of neurotransmission (Duan et al., 2015). Multiple models of MSC-mediated functional recovery of SCI through their paracrine activity at a single-gene level have been proposed over the years (Liau et al., 2020). However, little is known about the effect of hUC-MSC transplantation on the transcriptional regulation of ion channels and neurotransmitter receptors, which are key regulators of neuronal excitability, after SCI. To address this question, we characterized the hUC-MSC dose effect on the transcriptional regulation of 40 genes coding the main subunits of calcium and potassium channels, and of receptors of acetylcholine, glutamate, 5-hydroxytryptamine, dopamine, glycine, and GABA. We found that injury triggered the downregulation of most of the genes that we monitored and the hUC-MSCs induced gene expression recovery in a dose-dependent manner. Interestingly, only the two effective doses significantly restored the expression of all $GABA_A$ receptors, although the low dose elevated many transcripts, including *KCC2*. GABA is the major inhibitory neurotransmitter in the adult spinal cord. The hyperpolarizing action of $GABA_A$ receptors in mature neurons is under the control of a low intracellular Cl^- concentration maintained by the Cl^- extruder, KCC2. Several neurological disorders are associated with KCC2 deficiency, which compromises neurotransmission and results in hyperexcitability of neuronal networks (Medina et al., 2014). Boulenguez et al. (2010) have reported that KCC2 is downregulated after SCI in rats, particularly in motoneuron membranes, which is associated with spasticity. Using a mouse model of double hemisection SCI, a recent report has linked functional recovery with restoration of KCC2 expression in inhibitory neurons using the KCC2 agonist CLP290 or AAV-mediated overexpression in interneurons (Chen et al., 2018). Wienecke et al. (2010) have analyzed the global gene expression of rodent motor neurons following chronic SCI and found that most of the regulated genes coding for $GABA_A$ receptors were downregulated, which may be associated with the development of postinjury spasticity. Furthermore, a study on the lamprey model of SCI pointed out the possible roles of GABA receptors in neuroprotection and regeneration after injury (Romaus-Sanjurjo et al., 2018). The $GABA_A$ receptors are pentameric complexes assembled from 19 genes to form the chloride ion channel in limited combinations. Although the α1β2γ2 combination represents the largest population of $GABA_A$ receptors in the human brain (Zhu et al., 2018), the α2β3γ2 and α3β3γ2 combinations are the preponderant ones in the spinal cord (Fritschy et al., 2003). Our results revealed that both the effective doses of hUC-MSCs, but not the low dose, significantly upregulated all the subunits of $GABA_A$ receptors after SCI. Although the gene expression in the spinal cord tissue at the lesion site did not pinpoint the cell type of interest, the ubiquitous expression of GABAA receptors in neuronal cells of the CNS may provide a hint. The results suggest that the effect of hUC-MSCs on the activation of inhibitory $GABA_A$ receptors together with the K^+/Cl^- cotransporter KCC2 to inhibit neuronal excitability may be, in part, responsible for the reestablishment of damaged neural circuits. However, to our knowledge, it remains unknown whether the manipulation of the expression of $GABA_A$ receptors can improve the functional recovery of mammals after SCI, despite plenty of studies highlighting their roles in neuropathic pain (Gwak and Hulsebosch, 2011). If they can, how hUC-MSCs influence the expression of $GABA_A$ receptors in neurons remains to be characterized in future work. Our data indicate that $GABA_A$ receptors are strong candidates for therapeutic targeting of dormant relay pathways in injured spinal cord.

Regarding cell survival and differentiation of infused hUC-MSCs, it is technically feasible to monitor the GFP-labeled hUC-MSCs *in vivo* by lentiviral transduction. However, we did not detect the graft in the damaged spinal cord at 4-weeks post transplantation (data not shown), which is consistent with our previous observation that the longevity of the majority of the infused hUC-MSCs in the spinal cord was not longer than 1 week after injection (Yang et al., 2020b). The short lifespan of transplanted hUC-MSCs in a rat model is mainly because the xenografts elicit immunological rejection; hence, we applied immunosuppressant cyclosporine A during the entire experimental period. However, this should not be an issue of concern when we apply repeated subarachnoid administration of allogeneic hUC-MSCs in clinical trials.

We are aware of the limitations of our study. First, regarding the animal model of SCI, it would be better to use nonhuman primates, such as rhesus monkeys, rather than rats to evaluate the dose effects. Regarding the CST regeneration, the main descending tract in rodents is the dorsal tract in the ventral part of the dorsal column, which is distinct from a dorsolateral tract in humans. Second, the hUC-MSC doses tested are relatively limited, while preclinical studies generally require a stem cell dose escalation test, in which much higher doses need to be tested. As we mentioned before, we tested a relatively limited dose range mainly because previously we found that 4×10^6 hUC-MSCs/kg is safe and efficient for the treatment of subacute SCI through intrathecal implantation in rat models (Yang et al., 2020b).

To conclude, the dose of 1×10^6 hUC-MSCs/kg, but not the lower dose of 0.25×10^6 hUC-MSCs/kg, was as efficient as 4×10^6 hUC-MSCs/kg to improve functional recovery in a rat model of subacute SCI. Our results indicate that further investigation of GABAA receptors as possible therapeutic targets should be conducted.

Acknowledgments: *We deeply thank Wei-Wei Zou from Department of Cell Biology, School of Basic Medical Sciences, Southern Medical University for isolating hUC-MSCs and collecting samples. We thank the Third Affiliated Hospital of Sun Yat-sen University for their intrathecal injection of hUC-MSCs in patients with subacute SCI treatment registered in ClinicalTrials.gov (Identifier: NCT03521336).*

Author contributions: *TTC, HC and MML conceived the experimental design and wrote the manuscript. HQW performed MRI-DTI imaging. TTC, HC, MP and SSX conducted the rest of experiments and performed statistical analyses. BL and LMR provided professional consultation in clinical research. All authors approved the final version of the manuscript.*

Conflicts of interest: *The authors declare no competing financial interests.*

References

Boulenguez P, Liabeuf S, Bos R, Bras H, Jean-Xavier C, Brocard C, Stil A, Darbon P, Cattaert D, Delpire E, Marsala M, Vinay L (2010) Down-regulation of the potassium-chloride cotransporter KCC2 contributes to spasticity after spinal cord injury. Nat Med 16:302-307.

Chen B, Li Y, Yu B, Zhang Z, Brommer B, Williams PR, Liu Y, Hegarty SV, Zhou S, Zhu J, Guo H, Lu Y, Zhang Y, Gu X, He Z (2018) Reactivation of dormant relay pathways in injured spinal cord by KCC2 manipulations. Cell 174:1599.

Chen G, Fang X, Yu M (2015) Regulation of gene expression in rats with spinal cord injury based on microarray data. Mol Med Rep 12:2465-2472.

Chen K, Deng S, Lu H, Zheng Y, Yang G, Kim D, Cao Q, Wu JQ (2013) RNA-seq characterization of spinal cord injury transcriptome in acute/subacute phases: a resource for understanding the pathology at the systems level. PLoS One 8:e72567.

Cofano F, Boido M, Monticelli M, Zenga F, Ducati A, Vercelli A, Garbossa D (2019) Mesenchymal stem cells for spinal cord injury: current options, limitations, and future of cell therapy. Int J Mol Sci 20:2698.

Davies JE, Walker JT, Keating A (2017) Concise review: Wharton's jelly: the rich, but enigmatic, source of mesenchymal stromal cells. Stem Cells Transl Med 6:1620-1630.

Dolan EJ, Tator CH (1979) A new method for testing the force of clips for aneurysms or experimental spinal cord compression. J Neurosurg 51:229-233.

Dos Santos Ramalho B, Marques Pestana F, Andrade Prins C, Soares Dos Santos Cardoso F, Rufino Cavalcante D, Augusto Lopes de Souza S, Gutfilen B, Martins de Almeida F, Blanco Martinez AM (2019) Effects of different doses of mesenchymal stem cells on functional recovery after compressive spinal-cord injury in mice. Neuroscience 400:17-32.

Duan H, Ge W, Zhang A, Xi Y, Chen Z, Luo D, Cheng Y, Fan KS, Horvath S, Sofroniew MV, Cheng L, Yang Z, Sun YE, Li X (2015) Transcriptome analyses reveal molecular mechanisms underlying functional recovery after spinal cord injury. Proc Natl Acad Sci U S A 112:13360-13365.

Fan B, Wei Z, Yao X, Shi G, Cheng X, Zhou X, Zhou H, Ning G, Kong X, Feng S (2018) Microenvironment imbalance of spinal cord injury. Cell Transplant 27:853-866.

Fink KL, Cafferty WB (2016) Reorganization of intact descending motor circuits to replace lost connections after injury. Neurotherapeutics 13:370-381.

Fischer UM, Harting MT, Jimenez F, Monzon-Posadas WO, Xue HS, Savitz SI, Laine GA, Cox CS (2009) Pulmonary passage is a major obstacle for intravenous stem cell delivery: the pulmonary first-pass effect. Stem Cells Dev 18:683-691.

Forgione N, Karadimas SK, Foltz WD, Satkunendrarajah K, Lip A, Fehlings MG (2014) Bilateral contusion-compression model of incomplete traumatic cervical spinal cord injury. J Neurotraum 31:1776-1788.

Fritschy JM, Schweizer C, Brunig I, Luscher B (2003) Pre- and post-synaptic mechanisms regulating the clustering of type A gamma-aminobutyric acid receptors (GABAA receptors). Biochem Soc Trans 31:889-892.

Gwak YS, Hulsebosch CE (2011) GABA and central neuropathic pain following spinal cord injury. Neuropharmacology 60:799-808.

Han Q, Xie Y, Ordaz JD, Huh AJ, Huang N, Wu W, Liu N, Chamberlain KA, Sheng ZH, Xu XM (2020) Restoring cellular energetics promotes axonal regeneration and functional recovery after spinal cord injury. Cell Metab 31:623-641.e628.

Iwai H, Shimada H, Nishimura S, Kobayashi Y, Itakura G, Hori K, Hikishima K, Ebise H, Negishi N, Shibata S, Habu S, Toyama Y, Nakamura M, Okano H (2015) Allogeneic neural stem/progenitor cells derived from embryonic stem cells promote functional recovery after transplantation into injured spinal cord of nonhuman primates. Stem Cell Transl Med 4:708-719.

Joshi M, Fehlings MG (2002) Development and characterization of a novel, graded model of clip compressive spinal cord injury in the mouse: Part 1. Clip design, behavioral outcomes, and histopathology. J Neurotrauma 19:175-190.

Kabat M, Bobkov I, Kumar S, Grumet M (2020) Trends in mesenchymal stem cell clinical trials 2004-2018: Is efficacy optimal in a narrow dose range? Stem Cells Transl Med 9:17-27.

Krupa P, Vackova I, Ruzicka J, Zaviskova K, Dubisova J, Koci Z, Turnovcova K, Urdzikova LM, Kubinova S, Rehak S, Jendelova P (2018) The effect of human mesenchymal stem cells derived from Wharton's Jelly in spinal cord injury treatment is dose-dependent and can be facilitated by repeated application. Int J Mol Sci 19:1503.

Li MM, He YL, Dubois W, Wu XL, Shi JX, Huang J (2012) Distinct regulatory mechanisms and functions for p53-activated and p53-repressed dna damage response genes in embryonic stem cells. Mol Cell 46:30-42.

Li Y, Shen PP, Wang B (2021) Induced pluripotent stem cell technology for spinal cord injury: a promising alternative therapy. Neural Regen Res 16:1500-1509.

Liau LL, Looi QH, Chia WC, Subramaniam T, Ng MH, Law JX (2020) Treatment of spinal cord injury with mesenchymal stem cells. Cell Biosci 10:112.

Liu AM, Chen BL, Yu LT, Liu T, Shi LL, Yu PP, Qu YB, So KF, Zhou LB (2020) Human adipose tissue- and umbilical cord-derived stem cells: which is a better alternative to treat spinal cord injury? Neural Regen Res 15:2306-2317.

Medina I, Friedel P, Rivera C, Kahle KT, Kourdougli N, Uvarov P, Pellegrino C (2014) Current view on the functional regulation of the neuronal K+-Cl- cotransporter KCC2. Front Cell Neurosci 8:27.

Nagamura-Inoue T, He H (2014) Umbilical cord-derived mesenchymal stem cells: Their advantages and potential clinical utility. World J Stem Cells 6:195-202.

Percie du Sert N et al. (2020) Reporting animal research: Explanation and elaboration for the ARRIVE guidelines 2.0. PLoS Biol 18:e3000411.

Rao JS, Zhao C, Zhang A, Duan H, Hao P, Wei RH, Shang J, Zhao W, Liu Z, Yu J, Fan KS, Tian Z, He Q, Song W, Yang Z, Sun YE, Li X (2018) NT3-chitosan enables de novo regeneration and functional recovery in monkeys after spinal cord injury. Proc Natl Acad Sci U S A 115:E5595-5604.

Rivlin AS, Tator CH (1978) Effect of duration of acute spinal cord compression in a new acute cord injury model in the rat. Surg Neurol 10:38-43.

Romaus-Sanjurjo D, Ledo-Garcia R, Fernandez-Lopez B, Hanslik K, Morgan JR, Barreiro-Iglesias A, Rodicio MC (2018) GABA promotes survival and axonal regeneration in identifiable descending neurons after spinal cord injury in larval lampreys. Cell Death Dis 9:663.

Schneider CA, Rasband WS, Eliceiri KW (2012) NIH Image to ImageJ: 25 years of image analysis. Nat Methods 9:671-675.

Shende P, Subedi M (2017) Pathophysiology, mechanisms and applications of mesenchymal stem cells for the treatment of spinal cord injury. Biomed Pharmacother 91:693-706.

Shi LL, Zhang N, Xie XM, Chen YJ, Wang R, Shen L, Zhou JS, Hu JG, Lu HZ (2017) Transcriptome profile of rat genes in injured spinal cord at different stages by RNA-sequencing. BMC Genomics 18:173.

Silvestro S, Bramanti P, Trubiani O, Mazzon E (2020) Stem cells therapy for spinal cord injury: an overview of clinical trials. Int J Mol Sci 21:659.

Squair JW, Tigchelaar S, Moon KM, Liu J, Tetzlaff W, Kwon BK, Krassioukov AV, West CR, Foster LJ, Skinnider MA (2018) Integrated systems analysis reveals conserved gene networks underlying response to spinal cord injury. Elife 7:e39188.

Torres-Espin A, Corona-Quintanilla DL, Fores J, Allodi I, Gonzalez F, Udina E, Navarro X (2013) Neuroprotection and axonal regeneration after lumbar ventral root avulsion by re-implantation and mesenchymal stem cells transplant combined therapy. Neurotherapeutics 10:354-368.

Wienecke J, Westerdahl AC, Hultborn H, Kiehn O, Ryge J (2010) Global gene expression analysis of rodent motor neurons following spinal cord injury associates molecular mechanisms with development of postinjury spasticity. J Neurophysiol 103:761-778.

Yang Y, Pang M, Chen YY, Zhang LM, Liu H, Tan J, Liu B, Rong LM (2020a) Human umbilical cord mesenchymal stem cells to treat spinal cord injury in the early chronic phase: study protocol for a prospective, multicenter, randomized, placebo-controlled, single-blinded clinical trial. Neural Regen Res 15:1532-1538.

Yang Y, Pang M, Du C, Liu ZY, Chen ZH, Wang NX, Zhang LM, Chen YY, Mo J, Dong JW, Xie PG, Wang QY, Liu B, Rong LM (2021) Repeated subarachnoid administrations of allogeneic human umbilical cord mesenchymal stem cells for spinal cord injury: a phase 1/2 pilot study. Cytotherapy 23:57-64.

Yang Y, Cao TT, Tian ZM, Gao H, Wen HQ, Pang M, He WJ, Wang NX, Chen YY, Wang Y, Li H, Lin JW, Kang Z, Li MM, Liu B, Rong LM (2020b) Subarachnoid transplantation of human umbilical cord mesenchymal stem cell in rodent model with subacute incomplete spinal cord injury: Preclinical safety and efficacy study. Exp Cell Res 395:112184.

Zhao SJ, Zhou W, Chen J, Luo YJ, Yin GY (2018) Bioinformatics analysis of the molecular mechanisms underlying traumatic spinal cord injury. Mol Med Rep 17:8484-8492.

Zhou ZL, Mo BL, Qiu SJ, Chao D, Shi BC, Shuai H, Shun Y, Hui Z (2016) Preconditioning in lowered oxygen enhances the therapeutic potential of human umbilical mesenchymal stem cells in a rat model of spinal cord injury. Brain Res 1642:426-435.

Zhu S, Noviello CM, Teng J, Walsh RM, Jr., Kim JJ, Hibbs RE (2018) Structure of a human synaptic GABAA receptor. Nature 559:67-72.

Zukor K, Belin S, Wang C, Keelan N, Wang X, He Z (2013) Short hairpin RNA against PTEN enhances regenerative growth of corticospinal tract axons after spinal cord injury. J Neurosci 33:15350-15361.

C-Editors: Zhao M; S-Editor: Li CH; L-Editors: Li CH, Song LP; T-Editor: Jia Y